An Optimal Deep Wavelet Autoencoder-Based DNN with the use of Rider Cuckoo Search Algorithm for classification of the lung cancer on CT images

R. Tamilarasi
Research Scholar, Department of Computer Science, University of Madras, Chennai-600025

Dr. S. Gopinathan
Professor, Department of Computer Science, University of Madras, Chennai-600025

Abstract

The only way to enhance a patient's survival chances is to recognize the lung cancer early. A CT scan is utilized to determine the spot of a tumour and the extent of illness in the body. The CT scan of lung images was analysed in this study using an Optimal Deep Wavelet Autoencoder-Based DNN (ODWADNN). Using the Accelerated Greedy Snake's algorithm, a highly accurate, dependable, fast, automated paradigm was utilized to segment the liver tumour image (AGSA). In this case, the recommended RCSA is utilized to train the DBN. The recommended RCSA combines the ROAand the Cuckoo Search algorithm (CS). The discussed paradigm enhances the mentioned disease prediction rate, measured by MATLAB-based outcomes such as Reliability, Specificity, Precision, Recall, and F1 score.

Keywords: *the mentioned disease, Computed Tomography, Optimal Deep Wavelet Autoencoder-Based DNN, Segmentation, Accelerated Greedy snake's algorithm, ROA and CS.*

1. INTRODUCTION

The mentioned disease kills over one million people annually [1]. Early identification of this disease may limit mortality and increase patient survival when curative treatment is available. The doctor uses CT images to examine and predict the disease [2]. However, in many cases, a physician cannot make an accurate diagnosis without the aid of a CAD system.

For 2020, the projected incidence of illness patients in India was 679,421 (94.1 per 100,000) for males and 712,758 (103.6 per 100,000) for females. One in every 68 men (the mentioned disease), one in every 29 women (breast illness), and one in every nine Indians will form illness later in life (0-74 years of age) [3] if illness is recognized in its early stages, the chances of survival increase. Early identification of the mentioned disease is a difficult task. Around 80% of patients are effectively predicted only in the advanced or terminal stages of illness [5]. The mentioned disease is the second most common illness in men and the tenth most common illness in women [4]. After breast and colorectal illnesss, the mentioned disease is the third common disease in women [5]. One of image processing's simplest and most efficient dimensionality reduction paradigms is feature extraction [6]. The non-intrusive nature of CT imaging is one of its most notable characteristics [7]. The selected or retrieved characteristics will retrieve the appropriate details from the input data to the reduction operation [8]. Neural network paradigms with binarization image pre-processing are utilized for the mentioned disease image categorization [9].

Current studies for the mentioned disease categorization utilized a neural network paradigm that provided an reliability of 80%. Several studies have been conducted on the mentioned disease categorization and Classifiers, such as 'SVM, KNN, and ANN' [10]. Although, these paradigms are costly and only recognize the mentioned disease in its advanced stages, resulting in a meagre chance of survival. On the other hand, early identification of illness can aid in the complete cure of the disease. With this motivation, this study attempts to use deep learning and metaheuristic paradigms to provide a more efficient paradigm for the mentioned disease diagnosis. The following are the main accomplishments of the present research:

- • Introducing a novel paradigm for predicting the mentioned disease using CT scan images of the lungs.
- • Developing a new structure for the ODWADNN as a valuable tool for illness diagnosis.
- • Metaheuristic-based optimization of the convolutional neural network, the ROA and CS.
- • The AGSA is utilized to segment the tumour area in the liver image

At last, the defined intelligent technique-based illness identification system is implemented using the MATLAB tool, and the system's efficiency is ascertained using various efficiency metrics. Based on the preceding analysis, the work is organised. Section 2 briefs the related work on the mentioned disease identification. Section 3 briefs the paradigm for developing the recommended ODWADNN-based the mentioned disease identification operation. Section 4 provides simulation outcomes to depict the effciency of the recommended paradigm. Section 5 includes conclusions and recommendations for upcoming research.

2. Related work

Sheway et al. [11] utilized linear SVM, logistic regression, k-Nearest Neighbor (kNN), random forest, and AdaBoost classifiers to categorize nodules. Firmino et al. [12] utilized a rule-based classifier and SVM to categorize nodules. They utilized the LIDC-IDRI database [13] and got 97 % and 94.4 % recall. [14] established an ANN-based CT illness categorization. The statistical paradigm was developed for categorization. There is more reliability in backpropagation networks than in forwarding propagation networks.

[15] recommended a two-path CNN with "denoising first" (DFD-Net). It was discovered that this type of paradigm efficiently limits noise in an image, and is easily adaptable to nodule shape and size inconsistency. [16], a novel automated pulmonary nodule identification paradigm is based on modified V-Nets and a high-level descriptor-based SVM classifier. [17] recommended an efficient lung nodule identification paradigm based on multigroup patches retrieved from lung images and boosted with the Frangi filter.

In [18], researchers recommended an boosted multidimensional area-based fully convolutional network (mRFCN)-based automated decision support system for lung nodule identification and categorization. In [19], researchers recommended using transferable texture CNN to enhance the categorization of pulmonary nodules in CT scans. Nasrullah et al. [20] recommended a deep CNN-based Customized Mixed Link Network (CMixNet) paradigm for lung nodule identification and categorization. [21] recommended a deep learning paradigm to detect the mentioned disease from CT images for patients at Shandong Provincial Hospital. We use densely connected convolutional networks (DenseNet) to categorize malignant tumours from images acquired from, and AdaBoost algorithm to integrate multiple categorization outcomes to enhance categorization efficiency.

Recommend a CNN-based approach in [22] that uses MIP images of different slab thicknesses (5, 10, 15, etc.). In [23], the vesselness filter identifies lung nodules using Multi-Scene Deep Learning Architecture (MSDLF). This work suggests a new optimal deep learning paradigm with effective segmentation for lung nodule identification to overcome the above surveys.

3. Proposed Methodology

The recommended paradigm is utilized to categorize CT images of the human lung and includes several stages, including pre-operationing, segmentation, and finally, categorization. The infected area is divided using GSA from the noise-free lung CT image. The divided area is then utilized in the recommended categorizeing DNN paradigm to retrieve high-level characteristics for CT images using a deep wavelet auto encode to limit computational time and cost. The Optimal Deep Wavelet Autoencoder-Based DNN (ODWADNN) classifier was utilized in this study, and RCSA was utilized to optimise the structure. The categorisation problem is generally divided into two stages: training and testing. exThis paradigm is depicted in Fig. 1.

Fig.1.General diagram of recommended ODWADNN based The mentioned disease identification

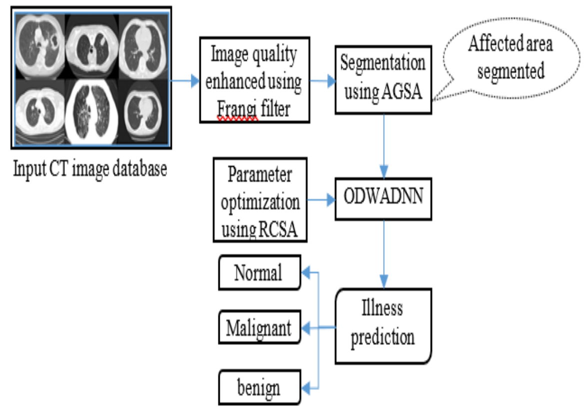

3.1 Data set Preparation

A LIDC/IDRI that includes 1018 helical thoracic CT scans from 1010 different patients is utilized. Four radiologists worked together in two stages to annotate the nodules in the LIDC/IDRI database. Each radiologist individually analysed the exams in the first stage. The four analyses from the first stage were presented to the four radiologists in the second stage. Each radiologist independently re-analyzed the exams and made their annotations [24]. Lung CT images were preserved in the DICOM format, and slice thickness and pixel spacing, can be validated [25]. The standardised pixel spacing was set to 0.688 mm, the mean of all pixel spacing values. Radiologists classified the nodules they annotated into small nodules with diameters less than 3mm and large nodules greater than 3mm. In this study, 1006 cases contained a total of 25723 two-dimensional nodules (>3mm) in these CT slices.

3.2 Frangi filter for image quality enhancement

In a CT scan of the lungs, vessels had a distinct morphology and structure from lung nodules. Lung nodules resembled ellipses, irregular spheres, or cotton-like structures. This step removed vascular structures in the lung, allowing us to analyse nodule-like structures better. The Frangi filter is the gold standard for vascular enhancement, enhancing vessel-like structures while weakening other structures [36]. Using a multi-scale Frangi filter, this study designed a paradigm to remove vascular structures from the lung. As was described in [32], one image $I(x,y)$, can be defined as a Taylor expansion in the neighbourhood of a random point $rp(x_0,y_0)$. The second-order term of the Taylor expansion contained the Hessian matrix of $I(x,y)$, which is indicated as $Hm_{rp,\sigma}$. Here rp defines $rp(x_0,y_0)$ and σ are indicated as the Gaussian kernel $Gk(x,y)$ scale, defined as (2). Thus $Hm_{rp,\sigma}$ can be computed by (1) and (2). $Hm_{rp,\sigma}$ is a matrix that includes the convolutions of the image $I(x,y)$ and the second-order differential of $Gk(x,y)$ concerning x or y.

$$Hm_{rp,\sigma} = \begin{bmatrix} I(x,y)\otimes\left(\frac{\partial}{\partial x}\right)\left(\frac{\partial}{\partial x}\right)Gk(x,y) & I(x,y)\otimes\left(\frac{\partial}{\partial x}\right)\left(\frac{\partial}{\partial y}\right)Gk(x,y) \\ I(x,y)\otimes\left(\frac{\partial}{\partial x}\right)\left(\frac{\partial}{\partial y}\right)Gk(x,y) & I(x,y)\otimes\left(\frac{\partial}{\partial y}\right)\left(\frac{\partial}{\partial y}\right)Gk(x,y) \end{bmatrix} \quad (1)$$

$$Gk(x,y) = \left(\frac{1}{2\pi\sigma^2}\right)\cdot exp(-\|x,y\|^2/2\sigma^2) \quad (2)$$

We, therefore, get the Hessian matrix $Hm_{rp,\sigma}$. The eigenvalues and eigenvectors of $Hm_{rp,\sigma}$, which are indicated as $Eval$ and $Evec$ $(k = 1,2)$ respectively, are both computed under the scale of σ. For a two-dimensional (2D) image, two eigenvalues ($Eval_1$ and $Eval_2$) indicate different identification structures. $Evec_1$ defines the direction along the vessel, and $Evec_2$ is the orthogonal direction of $Evec_1$. $Eval_1$ and $Eval_2$ play a decisive role in discriminating local vascular orientation. To recognize the bright vessel-like structure, $Eval_1$ and $Eval_2$ should fulfil two criteria:

$$|Eval_1| \approx 0\,; |Eval_1| \ll |Eval_2| \quad (3)$$

The measure formula of vessel likeliness Vl is displayed in (4) by using the two eigenvalues ($Eval_1$ and $Eval_2$).

$$Vl_{rp} = \begin{cases} 0 & if Eval_2 > 0 \\ \complement & otherwise \end{cases} \quad (4)$$

$$\complement = \exp\left(\frac{-|Eval_1/Eval_2|^2}{2th_1^2}\right)\left(\frac{1-\exp\|(Eval_1,Eval_2)\|^2}{2th_2^2}\right) \quad (5)$$

Where $\complement$ is a parameter to denote the formula of (5). The attributes th_1 and th_2 are adjustable thresholds that can control the filters' sensitivity to $|Eval_1/Eval_2|$ is important for differentiating the vessel-like and nodule-like structures, and 2-norm $\|(Eval_1,Eval_2)\|\cdot|Eval_1/Eval_2|$can reflect the contrast of the object and the background. According to the grayscale of images utilized in this study, th_1 and th_2were set to 0.6 and 20, respectively. First, the Frangi filter was utilized to create the vessel structure image. Then, two images were created: one of generated vessel structure and one of the lungs. When scale σ was set to 1.5, the vessel-like structures were virtually deleted, and the distortion of nodule-like structures was virtually eliminated.

3.3 Segmentation using AGSA

The recommended study utilized the fast greedy snake's algorithm to segment liver CT images. This algorithm utilized control points to fix the initial contour curve. Internal energy and curvature were obtained from the image gradient. The greedy snake algorithm includes energy function Eas shown in Eq. (6)

$$E = \sum_{i=1}^{N} \alpha_i E_{countinuity}(cp_i) + \beta_i\, E_{curvature}(cp_i) + L_{counteracting}(cp_i) \quad (6)$$

In which α_i, β_i and γ_i are weighing factors, $cp_i(i = 1,2, \dots N)$ defines all of the control points of the contour curve. The image energy ($L_{counteracting}$) is the external energy derived from the input image. The image contour is indicateed by pixels with arc lengths less than one. By selecting the neighbourhood pixel, the arc length is limited. The continuity energy is computed using the first-order continuity function shown in Eq. (7)

$$E_{countinuity}(cp_{i,j}) = \frac{Dist_{avg} - Dist_{cp_i - cp_{(i+1,j)}}}{\max\left(Dist_{avg} - Dist_{cp_i - cp_{(i+1,j)}}\right)} \quad (7)$$

$Dist_{cp_i - cp_{(i+1,j)}}$ is the distance between two consecutive pixels and $Dist_{avg}$ is the average distance between the adjacent pixels. It is the distance distribution between adjacent pixels of the contour. Dist_avgis is upgraded when the distance between adjacent pixels approaches davr. This helps the arc's pixels be evenly spaced. This energy determines how far the arc should bend to reach the concavity. Curvature energy is computed using Eq. (8)

$$E_{curvature}(cp_{i,j}) = \frac{cp_{i-1} - 2cp_{i,j} + cp_{i+1}}{\max(cp_{i-1} - 2cp_{i,j} + cp_{i+1})} \quad (8)$$

The largest values normalize the energy terms in the neighbourhood. Counteracting energy is de¯ned based on the local gradient energy given by Eq. (9)

$$L_{counteracting}(cp_{i,j}) = \frac{I(cp_{i,j})}{\max\left(I(cp_{i,j})\right) - \min\left(I(cp_{i,j})\right)} \quad (9)$$

where $I(cp_{i,j})$ is the intensity gradient. According to the equation above, moving the arc limited the total energy. The algorithm finds the next pixel cross pattern and diagonal pattern. Each iteration swaps these two patterns to limit computation time and enhance segmentation reliability.

3.4 The mentioned disease prediction using ODWADNN

A DWA can retrieve and learn principal components from large data distributions. This technique was utilized as an image compression and feature selection technique in this study. The middle layer includes the encoded image with a 64×64 size. Mathematically let X_i defines the divided input, H_i defines Hidden Layer (here I is 1 to 3), and Y_i defines the outcome. Let the activation functions af utilized I as depicted in eq (10):

$$H_i = af_i(W_i X_i + b_i), i = 1,2,3,4 \quad (10)$$

W_i is the weight vector between X_i to H_1, H_1 to H_2 and Y_i. The sparse Autoencoder [27] has a higher amount of hidden units than input units. Mathematically, the basic sparse Autoencoder includes a single hidden layer, H, connected to the input vector, v, with a weight matrix w. The outcome is created from the hidden layer as a reconstructed vector, v', that uses a new weight matrix nw. The bias is indicated as $bias$, and the activation function is slated as af . The formulation is indicated below in eq. (11)

$$X = af(W_v + bias); v' = af(W'X + bias') \quad (11)$$

The learning operation for the error propagation is stated below in eq.(12):

$$\min \|v - v'\|_2^2 \quad (12)$$

Fig.2. A architecture of a single layer of Deep Wavelet Autoencoder.

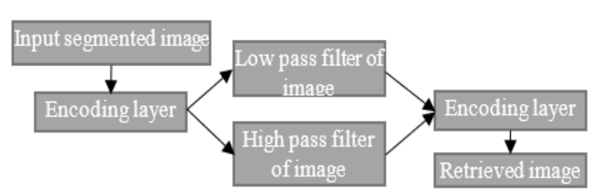

A single layer DWA architecture is shown in Fig.2. This architecture can be deepened. This technique uses a DWT [28]. Only approximation coefficients are utilized for categorization in a DNN paradigm. Table 1 shows the DWA step-by-step algorithm.

Table 1. The step by step algorithm of DWA

Step 1. Segmentation of Lung CT images to retrieve the illness area only.
Step 2. Dividing of a dataset to sub arrays
Step 3. for each sub-array, continue the steps 4 to 8
Step 4. Provide the image sub-array to Deep Wavelet Autoencoder for encoding
Step 5. Transfer the encoded image via low and high pass filters by discrete wavelet transform for decomlocation.
Step 6. Employ inverse wavelet transform to integrate and decode the images to acquire the real image
Step 7. Operation the Autoencoder for the amount of epochs to acquire optimized weight and bias values
Step 8. Retrieve approximation coefficients from the hidden layer, integrate them and bring an input to a DNN for categorization.

3.5. Categorization of lung CT images

The present study suggested DNN in the CT image categorization paradigm. Following feature selection, DNN groups the resulting component vector. This classifier uses two capacities: deep DBN and RBM. An RCSA optimization is considered to enhance the recommended paradigm's categorization efficiency (see the section below for details).

Deep belief network: The DBN paradigm rewards the system for delivering precise starts based on its hidden unit conditions. A DBN's attributes are the layer weights and the layer bias. Setting up attributes to train DNN help of a restricted RBM [29].

Restricted Boltzmann machine (RBM): It is a two-layer rehashed neural architecture in which symmetrically-weighted affiliations link stochastic twofold sources of details. The class check is ignored in a preparation case, and the RBM condition is expanded stochastically (13). This vector is also reversed in RBM, resulting in confabulating (retrying) the remarkable data.

$$features(w,h) = -\sum_{i=1}^{i}\sum_{j=1}^{j} I_{ij} w_i h_j - \sum_{i=1}^{I}\alpha_i w_i - \sum_{j=1}^{J}\beta_j h_j \qquad (13)$$

Where I_{ij} defines the symmetric interaction term between the visible unit, w_i is the weight matrix. The hidden unit s hj, α, β are the bias terms, i, j are the numbers of visible and hidden units.

Training of RCSA based DBN: This section describes how to train the recommended RCSA-based DBN classifier. RCSA is utilized to train RCSA-based DBNs to choose the appropriate weights optimally. The MLP training operation is based on the RCSA algorithm and involves distributing training data.

Furthermore, RCSA is utilized to compute optimal weights, then evaluated using an error function. The recommended RCSA is created by combining ROA and CSA. ROA [30] is based on the concept of a group of riders racing to a specific spot. The cuckoo breed behaviour is utilized to develop the CS algorithm [31]. The RCSA is outlined below:

Initialization Operation. Initialize the weights in a random manner and is indicated as

$$w = \{w^1, \dots, w', \dots w^{\vartheta}\} \qquad (14)$$

In which w' defines the weight between input and hidden layers, and w^ϑ defines the weight between hidden and outcome layers.

Error computation. The error Err is computed based on the difference formed between the desired and the acquired outcomes and is indicated as,

$$Err_f = \frac{1}{u}\sum_{q=1}^{u}\left(OO^q - DO^q\right)^2, 1 \le u \qquad (15)$$

here OO^q shows the acquired outcome, and DO^q defines the desired outcome.

The equation for these are given below.

$$w_{q+1}^{B}(c,w) = \eta\left[w_q(l,w) * \lambda(w) + w_q(o,w) * [1-\lambda(w)]\right] \qquad (16)$$

here η shows a random number, l and o is a random number between 1 and R, and λ defines a random number ranging between [0,1]. The equation of the follower is given by

$$w_{q+1}^{F}(c,s) = w^{lr}(lr,s) + \left[\cos\left(v_{c,s}^{q} * w^{lr}(lr,s) * B_c^q\right)\right] \qquad (17)$$

here s is coordinate selector, w^{lr} defines the leading rider's spot, lr specifies the index of leading rider, 횢 $v_{c,s}^{q}$ defines the steering angle of cth rider in sth coordinate, and B_c^q is the distance traveled by cth rider. The overtaker upgrade is utilized in the weight upgrade operation to maximize the success rate and is given by

$$w_{q+1}^{o}(c,s) = w_q(c,s) + \left[\xi_q^*(c) * w^{lr}(lr,v)\right] \qquad (18)$$

where $\xi_q^*(c))$ indicate the direction indicator, $w_q(c,s)$ defines the spot of the cth rider in the vth coordinate. The attacker tends to take the leader's spot by updating the coordinates rather than the selected values, so the attacker's upgrade operation is given by

$$w_{q+1}(c,w) = w^{lr}(lr,s) + \left[\cos s_{c,s}^{q} * w^{lr}(lr,s)\right] + B_c^q \qquad (19)$$

Assuming the leading spot of ROA $w \quad (orld,s)$ be done using w_{q+1}, and thus, the equation is given by,

$$w_{q+1}^{c,w} = w_q^{c,w} + \kappa \otimes levy(v) = w^{lr}(lr,s) \qquad (20)$$

where $w_q^{c,w}$ defines the weight at current iteration, κ defines the step size, ⊗ defines the entry wise multiplication operator, and $levy(v)$defines the levy fight with dimension v. After substituting the above equation in Eq. (19), the final equation for recommended RCSA is given as,

$$w_{q+1}(c,w) = w^{lr}(lr,s)\left[1 + \cos s_{c,s}^{q}\right] + B_c^q \quad (21)$$

Use the fitness function to find a outcome. The outcomes are ranked based on fitness values computed by specificity, with the best outcome having the lowest fitness values. Stop the flow. The iteration is repeated until the optimal global outcome is generated. Fig.3 shows the recommended ODWADNN general architecture.

Fig.3.The general architecture of the recommended ODWADNN

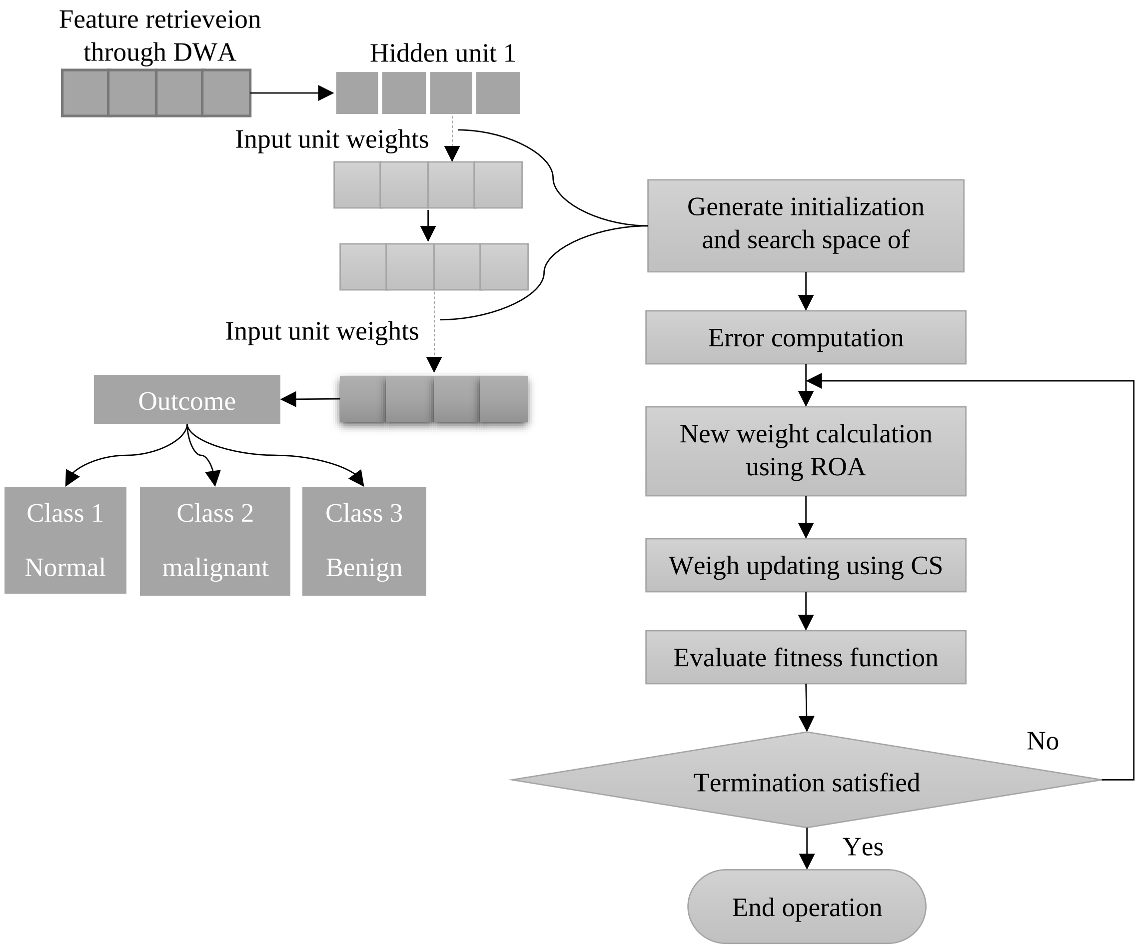

4. Experimental outcomes and discussion

This section assesses the boosted DNN and ensemble classifier-based the mentioned disease identification system. As previously stated, the system uses the LIDC-IDRI dataset during implementation. Comparing ODWADNN outcomes to SVM, KNN, ANN, mRFCN, and CNN. The recommended paradigm's efficiency is determined by its ability to recognize illnessous or nonillnessous lung images. The paradigm can predict a new patient's lung condition based on testing data.

Because the divided area is utilized to derive practical characteristics, its reliability must be evaluated. Table 4 shows the obtained outcomes.

$$\text{accuarcy} = \frac{TP+TN}{TP+TN+FP+FN} \qquad (22)$$

$$\text{specificity} = \frac{TN}{TN+FP} \qquad (23)$$

$$\text{Precision} = \frac{TP}{TP+FP} \qquad (24)$$

$$\text{Recall} = \frac{TP}{TP+FN} \qquad (25)$$

$$\text{F1 score} = 2 \times \frac{\text{precision}\times\text{recall}}{\text{precision}+\text{recall}} \qquad (26)$$

Metrics / Paradigms	KNN	ANN	SVM	mRFCN	CNN	ODWADNN
Reliability	0.72	0.84	0.87	0.88	0.91	0.96

Specificity	0.86	0.88	0.90	0.94	0.95	0.98
precision	0.87	0.88	0.91	0.92	0.94	0.97
Recall	0.84	0.87	0.86	0.87	0.91	0.98
F1score	0.83	0.87	0.88	0.89	0.93	0.98

4.1. Reliability comparison

Fig.4. Result of Reliability

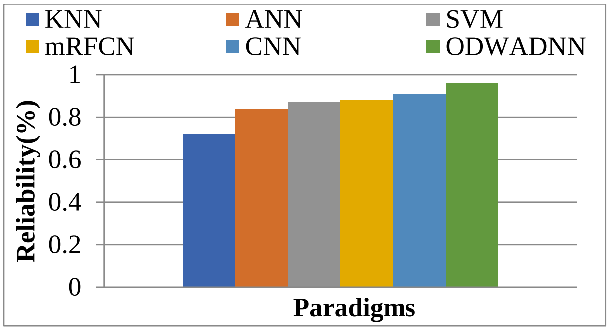

To compare recommended and traditional paradigms for feature count in databases, see Fig.4. The ODWADNN enhances reliability while speeding up operationing. Because it does not require many derived factors during pre-operationing, the ODWADNN has a 0.96 % reliability. In addition, the recommended system boosted illness identification using DWA-based feature reduction and image compression.

4.2. Specificity comparison

Fig.5. Result of Specificity

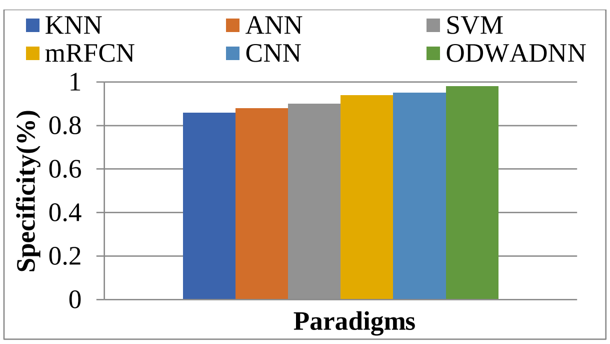

Fig.5 shows the reliability of recommended and traditional paradigms for feature count in given databases. The ODWADNN enhances reliability while speeding up operationing. Compared to other paradigms, the ODWADNN is 0.98 % accurate. When compared to traditional classifiers, the recommended ODWANN algorithm outperforms them. The analysis shows that DWA-based characteristics outperform other classifiers in identification reliability. Compared to other categorization paradigms, the ODWADNN classifier effectively identifies the mentioned disease.

4.3. Precision Rate comparison

Fig.6. Result of Precision

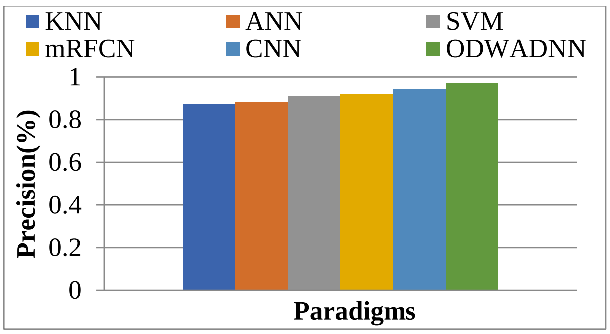

According to Fig.6, the precision of suggested and conventional paradigms for the amount of characteristics in given databases. While the amount of characteristics expands, so does the corresponding precision. In comparison to the traditional paradigms, the ODWADNN, for example, provides a precision of 0.97 %. This is because the ODWADNN does not require high-dimensional characteristics or derived factors and may discover a comparatively better-sorted collection of input within a given time interval. On the whole, the suggested categorization obtained good outcomes, and it was discovered that the system was able to handle this and enhance system efficiency.

4.4. Recall Rate comparison

Fig.7. Result of Recall

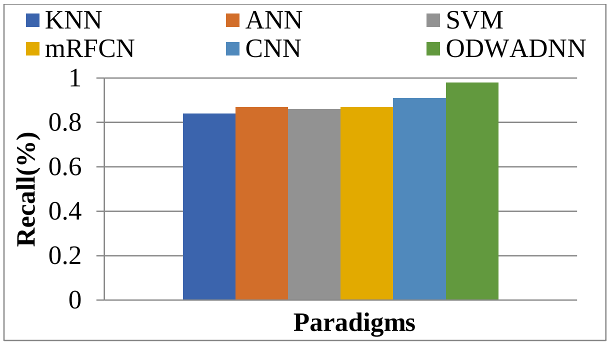

The recall of recommended and traditional paradigms for the amount of characteristics in a given database is shown in Fig.7. As the amount of characteristics accelerates, so does the recall. For example, when compared to traditional paradigms, the ODWADNN achieves a recall of 0.98 %. This is because the RCSA limits the computation time of the derived factors, allowing for the simplest fine-tuning of DWADNN. On the whole, the deep learning algorithms produced the best outcomes when it came to detecting the mentioned disease in CT images.

4.5. F-measure Rate comparison

Fig.8. Result of F-measure

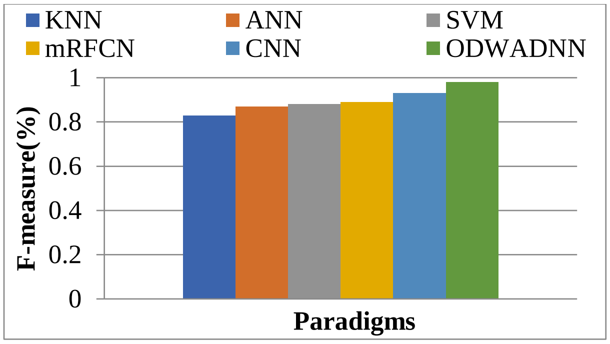

According to Fig.8, the f-measure of suggested and traditional paradigms for the amount of characteristics in provided databases. The f-measure is significantly boosted while the amount of characteristics is exceeded. For example, the ODWADNN has an f-measure of 0.98 % compared to all other paradigms. The DWA algorithm was utilized to find specific characteristics and compress images. As a result, additional operationing, memory requirements, and time complexity can be limited to fit the recommended paradigm in illness identification.

5. Conclusion and future work

When contrasted to other categorization paradigms, the suggested ODWADNN with segmentation performed better in the case of CT images. The divided area is effectively-recognized using AGSA, and various characteristics are retrieved that are prominent in dimension, requiring more time to recognize illness. An automatic the mentioned disease categorization paradigm limits manual labelling time and eliminates manual error. According to the outcomes of the experiments, the recommended technique is effective for categorizeing human lung images regarding reliability, specificity, precision, recall, and f-measure, with values of 0.96 %, 0.98 %, 0.97 %, 0.98 %, and 0.98 %, respectively. The reliability level has demonstrated that the recommended technique is effective in detecting illness-infected parts in CT images. The categorization outcomes demonstrate the benefits of this paradigm: it is quick, easy to use, non-invasive, and inexpensive. High-dose CT images and optimal feature selection are utilized to recognize this disease in future work.

Reference

C. Ridge, A. McErlean, and M. Ginsberg, “Epidemiology of The mentioned disease,” Semin. Intervent. Radiol., vol. 30, no. 2, pp. 093–098, May 2013.

Menezes, R. J., Roberts, H. C., Paul, N. S., McGregor, M., Chung, T. B., Patsios, D., ... & Shepherd, F. A. (2010). The mentioned disease screening using low-dose computed tomography in at-risk individuals: the Toronto experience. The mentioned disease, 67(2), 177-183.

Mathur, P., Sathishkumar, K., Chaturvedi, M., Das, P., Sudarshan, K. L., Santhappan, S., ... & ICMR-NCDIR-NCRP Investigator Group. (2020). Illness statistics, 2020: report from national illness registry programme, India. JCO Global Oncology, 6, 1063-1075.

D.U. Wutsqa, H.L.R. Mandadara, The mentioned disease classification using radial basis function neural network model with point operation, in: Image and Signal Operationing, BioMedical Engineering and Informatics (CISP-BMEI), 2017 10th International Congress on, IEEE, 2017, pp. 1–6.

D. Bhatnagar, A.K. Tiwari, V. Vijayarajan, A. Krishnamoorthy, Classification of Normal and Abnormal Images of The mentioned disease, in: IOP Conference Series: Materials Science and Engineering, vol. 263 (4), IOP Publishing, 2017, p. 042100.

B. El-Sherbiny, N. Nabil, S.H. El-Naby, Y. Emad, N. Ayman, T. Mohiy, A. AbdelRaouf, BLB (brain/the mentioned disease detection and segmentation and breast dense calculation), in: Deep and Indicateation Learning (IWDRL), 2018 First International Workshop on, IEEE, 2018, pp. 41–47.

F. Chen, D. Zhang, J. Wu, B. Zhang, Computerized analysis of tongue sublingual veins to detect lung and breast illnesss, in: Computer and Communications (ICCC), 2017 3rd IEEE International Conference on, IEEE, 2017, pp. 2708–2712.

Chaudhary, A., & Singh, S. S. (2012, September). The mentioned disease detection on CT images by using image operationing. In 2012 International Conference on Computing Sciences (pp. 142-146). IEEE.

Kuruvilla, J., & Gunavathi, K. (2014). The mentioned disease classification using neural networks for CT images. Computer paradigms and programs in biomedicine, 113(1), 202-209.

Günaydin, Ö., Günay, M., & Şengel, Ö. (2019, April). Comparison of the mentioned disease detection algorithms. In 2019 Scientific Meeting on Electrical-Electronics & Biomedical Engineering and Computer Science (EBBT) (pp. 1-4). IEEE.

T. Nesibu Shewaye and A. Ali Mekonnen, "Benign-malignant lung nodule classification with geometric and appearance histogram characteristics", arXiv:1605.08350, 2016,

M. Firmino, G. Angelo, H. Morais, M. R. Dantas and R. Valentim, "Computer-aided detection (CADe) and diagnosis (CADx) system for the mentioned disease with likelihood of malignancy", Biomed. Eng. OnLine, vol. 15, no. 1, pp. 2, Dec. 2016.

S. G. Armato et al., "The lung image database consortium (LIDC) and image database resource initiative (IDRI): A completed reference database of lung nodules on CT scans", Med. Phys., vol. 38, no. 2, pp. 915-931, Jan. 2011.

J. Kuruvilla, K. Gunavathi, The mentioned disease classification using neural networks for CT images, Comput. Paradigms Programs Biomed. 113 (1) (2014) 202–209.

Sori, W. J., Feng, J., Godana, A. W., Liu, S., & Gelmecha, D. J. (2021). DFD-Net: the mentioned disease detection from denoised CT scan image using deep learning.

Frontiers of Computer Science, 15(2), 1-13.

Ye, Y., Tian, M., Liu, Q., & Tai, H. M. (2020). Pulmonary Nodule Detection Using V-Net and High-Level Descriptor Based SVM Classifier. IEEE Access, 8, 176033-176041.

Jiang, H., Ma, H., Qian, W., Gao, M., & Li, Y. (2017). An automatic detection system of lung nodule based on multigroup patch-based deep learning network. IEEE journal of biomedical and health informatics, 22(4), 1227-1237.

Masood, A., Sheng, B., Yang, P., Li, P., Li, H., Kim, J., & Feng, D. D. (2020). Automated decision support system for the mentioned disease detection and classification via boosted RFCN with multilayer fusion RPN. IEEE Transactions on Industrial Informatics, 16(12), 7791-7801.

Ali, I., Muzammil, M., Haq, I. U., Khaliq, A. A., & Abdullah, S. (2020). Efficient lung nodule classification using transferable texture convolutional neural network. Ieee Access, 8, 175859-175870.

N. Nasrullah, J. Sang, M. S. Alam, M. Mateen, B. Cai and H. Hu, "Automated lung nodule detection and classification using deep learning combined with multiple paradigms", Sensors, vol. 19, no. 17, pp. 3722, Aug. 2019.

Pang, S., Zhang, Y., Ding, M., Wang, X., & Xie, X. (2019). A deep model for the mentioned disease type identification by densely connected convolutional networks and adaptive boosting. IEEE Access, 8, 4799-4805.

Zheng, S., Guo, J., Cui, X., Veldhuis, R. N., Oudkerk, M., & Van Ooijen, P. M. (2019). Automatic pulmonary nodule detection in CT scans using convolutional neural networks based on maximum intensity projection. IEEE transactions on medical imaging, 39(3), 797-805.

Zhang, Q., & Kong, X. (2020). Design of Automatic Lung Nodule Detection System Based on Multi-Scene Deep Learning Architecture. IEEE Access, 8, 90380-90389.

Y. LeCun, Y. Bengio, G. Hinton, "Deep learning," Nature, vol. 521, no. 7553, pp. 436–444, 2015.

S. G. Armato III, G. McLennan, L. Bidaut, M. F. McNitt-Gray, C. R. Meyer, A. P. Reeves, and E. A. Kazerooni, "The lung image database consortium (LIDC) and image database resource initiative (IDRI): a completed reference database of lung nodules on CT scans," Med. Phys., vol. 38, no. 2, pp. 915–931, 2011.

C.-Y. Liou, W.-C. Cheng, J.-W. Liou, and D.-R. Liou, ''Autoencoder for words,'' Neurocomputing, vol. 139, pp. 84–96, Sep. 2014.

Y. Xiao, J. Wu, Z. Lin, and X. Zhao, ''A semi-supervised deep learning paradigm based on stacked sparse auto-encoder for illness prediction using RNA-seq data,'' Comput. Paradigms Programs Biomed., vol. 166, pp. 99–105, Nov. 2018.

A. N. Akansu, W. A. Serdijn, and I. W. Selesnick, ''Wavelet transforms in signal operationing: A review of emerging applications,'' Phys. Commun. vol. 3, no. 1, pp. 1–18, 2010.

Ryu, S., Noh, J., & Kim, H. (2017). DNN based demand side short term load forecasting. Energies, 10(1), 3.

Binu D, Kariyappa BS (2018) RideNN: a new rider optimization algorithm-based neural network for fault diagnosis in analog circuits. IEEE Trans Instrum Meas 99:1–25

Gandomi AH, Yang XS, Alavi AH (2013) Cuckoo search algorithm: a metaheuristic approach to solve structural optimization problems. Eng Comput 29(1):17–35